Biochimica et Biophysica Acta 1838 (2014) 2778–2787

Contents lists available at ScienceDirect

Biochimica et Biophysica Acta

journal homepage: www.elsevier.com/locate/bbamem

Molecular dynamics simulations of histidine-containing cod antimicrobial peptide paralogs in self-assembled bilayers

Mohammad Hassan Khatami [a,1], Marek Bromberek [a], Ivan Saika-Voivod [a], Valerie Booth [a,b,*]

[a] Department of Physics and Physical Oceanography, Memorial University of Newfoundland, St. John's, NL A1B 3X7, Canada
[b] Department of Biochemistry, Memorial University of Newfoundland, St. John's, NL A1B 3X9, Canada

ARTICLE INFO

Article history:
Received 9 March 2014
Received in revised form 10 July 2014
Accepted 14 July 2014
Available online 21 July 2014

Keywords:
Antimicrobial peptide
POPC
Histidine
GROMACS
Molecular dynamics
Simulation

ABSTRACT

Gaduscidin-1 and -2 (GAD-1 and GAD-2) are antimicrobial peptides (AMPs) that contain several histidine residues and are thus expected to exhibit pH-dependent activity. In order to help elucidate their mechanism of membrane disruption, we have performed molecular dynamics simulations with the peptides in both histidine-charged and histidine-neutral forms, along with 1-palmitoyl-2-oleoyl-sn-glycero-3-phosphocholine (POPC) lipid molecules. The simulations employed GROMACS software and an OPLS-AA force field. Initially, the peptide and lipids were placed randomly in the simulation box and then were allowed to self-assemble. The results demonstrated a marked preference for the regions of the peptides that contain sequential pairs of histidine residues to associate closely with bilayer pores. This preference is observed even when the histidines are in their uncharged form. It appears that the relative compactness and rigidity of histidine pairs require the more aqueous and disordered environment of the pores to satisfy hydrophilic interactions. The final peptide structures exhibited a wide variety of structures and topologies, with the most helical structures positioning most parallel to the bilayer surface and the less ordered structures interacting more closely with the pore. Thus, the results give atomistic insight into those models of AMP mechanism that promote the importance of structural heterogeneity and imperfect amphipathicity to AMP activity and selectivity.

© 2014 Elsevier B.V. All rights reserved.

1. Introduction

Antimicrobial peptides (AMPs) play an important role in the immune systems of a wide variety of organisms, from humans to fish to insects. AMPs are generally amphipathic and cationic in nature (1), and consequently have a propensity to interact with lipid bilayers. Much of the research into the mechanism of AMPs has focused on their interaction with membranes, either as their direct mechanism of killing, or as a means of getting inside the cell to disrupt intracellular targets (2–5). Besides their natural roles in innate immunity, AMPs are also being investigated as potential therapeutics for conditions such as drug resistant infection (6–8) and cancer (9–11).

Many AMPs exhibit a degree of specificity and can kill pathogens at concentrations that do not harm host cells. At least some of this specificity is believed to derive from their cationic nature which provides for stronger interactions with, for example, bacterial or cancer cell membranes, which are generally more anionic in character than mammalian host cells (12,13). Nonetheless, one major barrier to using AMPs as drugs is that at high concentrations, they can kill not just the target cells but the healthy host cells as well (14,15).

One way of controlling the specificity and activity of AMPs is via controlling their charge. This is particularly applicable to peptides that contain the amino acid histidine, which is generally uncharged at neutral pH but tends to become positively charged at mildly acidic pH. This pH sensitivity of histidine-containing AMPs can provide a "pH switch" to activate them in lower pH environments (16–19). Acidic pH activation of AMPs may play a role in the endogenous functioning of AMPs; for example, acidic pH is important in skin immune defense (16,20). Moreover, there are intriguing possibilities to employ pH-activated AMPs in exogenous applications, such as the treatment of cancer (9,10) as the environment around tumors is usually acidic (17,21). Thus, histidine-containing AMPs are excellent candidates as therapeutics because they are likely to be much more active in the vicinity of the tumor than elsewhere in the body. Indeed, replacement of arginines and lysines with histidine in the AMP K6L6 was shown to make the peptide more specific; systemic injection of the modified peptide inhibited tumor growth in mice with reduced systemic toxicity compared to the parent peptide (17).

Abbreviations: GAD, Gaduscidin; AMP, antimicrobial peptide; POPC, 1-palmitoyl-2-oleoyl-sn-glycero-3-phosphocholine; GROMACS, GROningen MAchine for Chemical Simulations; SPV, Swiss PDB Viewer; DSSP, Define Secondary Structure of Proteins; VMD, Visual Molecular Dynamics; OPLS-AA, Optimized Potentials for Liquid Simulations-All Atom

* Corresponding author at: Department of Biochemistry, Memorial University of Newfoundland, St. John's, NL A1B 3X9, Canada. Tel.: +1 709 864 4523.
E-mail address: vbooth@mun.ca (V. Booth).
[1] First name is: Mohammad Hassan, last name is: Khatami.

http://dx.doi.org/10.1016/j.bbamem.2014.07.013
0005-2736/© 2014 Elsevier B.V. All rights reserved.

At least three different mechanisms have been suggested for the altered activity of histidine-containing AMPs that is observed when histidines become more positively charged at lower pH. 1) Membrane binding: Kacprzyk et al replaced the lysine and arginine in synthetic AMP sequences with histidines to produce peptides that were only active under acidic conditions (16). The differences in activity corresponded well to observed differences in membrane binding. 2) Membrane penetration: Kharadia et al also replaced the lysine and arginine residues in lytic peptides with histidines. They found that the novel peptides were much more selective for bacteria over host tissue cells and attributed the increase in activity at lower pH not to changes in membrane binding, but to increased membrane penetration (22). 3) Changing peptide structure: This mechanism for pH-dependent activity in histidine-containing AMPs was suggested by detailed studies of the synthetic peptide LAH4, for which pH alterations induce changes in the peptide structure. At neutral pH a long helix is formed, which associates with the membrane in a planar manner. At slightly acidic pH, a hinge disrupts the contiguous helix structure, possibly due to electrostatic repulsion between adjacent histidines (23).

We were interested in exploring, at an atomic level, the role of histidines in AMP-membrane interactions. Of particular interest were histidines in natural sequences as opposed to the synthetic sequences that have been the subjects of most mechanistic studies of histidine-containing AMPs so far. Additionally, we wanted to probe the potential significance of histidines that appear in sequential pairs in the sequence, as opposed to histidines flanked solely by non-histidine residues. The peptides employed in the study, GAD-1 and GAD-2, are derived from codfish sequence libraries (24–27). They are paralogs, i.e., related genes found in the same organism, and their comparison has potential to illuminate the role of histidine pairs in evolutionarily tuned structure–function relationships. GAD-1 and GAD-2 are members of the piscidin family of helical AMPs. Piscidins have been subjects of several structure–function studies, although not studies that address pH-dependent behavior and mechanisms (28–37). GAD-1 (FIHHIIGWISHGVRAIHRAIH-NH_2) has 5 histidines, two of which appear in a pair and three of which appear singly. GAD-2 (FLHHIVG LIHHGLSLFGDR-NH_2) has 4 histidines, which appear in two sets of histidine pairs. We studied these peptides in histidine charged forms, denoted as GAD-1p and GAD-2p, as well as in the histidine neutral form (GAD-1, GAD-2). All-atom molecular dynamics simulations with these 4 peptides along with POPC lipids were performed in order to reveal atomistic details of their lipid interactions. As detailed in the Methods and Discussion sections, with our system setup, pores form even in the absence of peptide, and thus our study does not provide a kinetic picture of how the peptides bind to membranes and induce pore formation, but rather provides details of the peptide/lipid interactions. One of our key findings was that histidine pairs are more likely to be found closely associated with the pore than in the more ordered, planer region of the lipid bilayers.

2. Methods

Our approach followed the method of Salgado et al. (38) who start unassembled lipid molecules in random positions with a single peptide among the lipid molecules. This method allows the system to freely assemble into a peptide–bilayer complex, thus avoiding any artifacts that might result from, for example, introducing the peptide into a pre-assembled bilayer after removing lipids "by hand". The main difference in our implementation of this approach is that, rather than employing a script to randomize the position of the lipids, we randomized the system by simulating at high temperature, 1400 K. This modification provided ease of implementation, in particular by allowing for an initial volume not too much larger than the final one, while avoiding truly unphysical interactions.

Salgado et al. (38) found that the method produced expected outcomes in terms of the location and orientation of the peptide with respect to the membrane, i.e., a hydrophobic peptide ended up in a transmembrane configuration, while a more amphipathic peptide ended up on and parallel to the membrane surface. This lends confidence that the assembled structures reflect low free energy states of the equilibrium system. By contrast to these two simpler cases, imperfectly amphipathic peptides, such as the ones we are studying, may possess many different configurations of similar free energy. To address this, for each system composition, we performed four independent simulations of the self-assembly process. While computational resources limited us to this small number, it did provide sufficient sampling for at least a semi-quantitative characterization of the differences between the paralogs in their charged and uncharged forms. Additionally, simulations were carried out in the absence of the peptide to control for the effect of the peptide on bilayer formation.

The systems consisted of 128 POPC lipid molecules (6656 atoms), a single peptide (~350 atoms) and approximately and no less than 7360 water molecules (roughly 37,000 atoms in total) (Table 1). This number of lipid molecules provided a large enough bilayer to accommodate the peptide in the presence of a pore. The amount of water was chosen to allow for sufficient space to prevent periodic boundary conditions from permitting the peptide to interact unphysically with both leaflets through water. The number of water molecules employed is somewhat larger than the number employed in other studies (38–40).

The initial alpha-helical peptide structures were generated using Swiss PDB Viewer (SPV) (41–44). The C-terminus was amidated with an NH_2 group to be in line with ongoing experimental work. The peptide was placed in a cubic simulation box of side length 8 nm along with the 128 POPC molecules, which were initially arranged in a bilayer configuration taken from (45) (Fig. 1A). Sufficient Cl^- counterions were added to ensure overall charge neutrality: 3 ions for GAD-1, 8 for GAD-1p, 1 for GAD-2 and 5 for GAD-2p. For histidines in GAD-1p and GAD-2p, the protonated form of histidine was used.

GROMACS version 4.5 was used for the simulations (46). We employed a version of the all atom Optimized Potential for Liquid Simulations (OPLS-AA) force field (47,48), adapted for POPC lipid molecule properties (49).

As the first step in generating randomized starting configurations for the self-assembly process, we carried out a simulation of the system comprising the peptide, lipid bilayer and counter ions in the canonical ensemble at T = 1400 K for 2 ns, still within a cubic box of side length 8 nm, while restraining the position of all the peptide atoms to preserve its helical structure. We employed the modified Berendsen thermostat (*v-rescale* in GROMACS). Under these conditions, the lipid bilayer immediately disassembles, equilibrating rapidly to a highly mobile fluid of lipid molecules (Fig. 1B). In this regime, the root mean square displacement of a lipid molecule over 1 ns is approximately 10 nm.

Next, we added approximately 7500 TIP4P water molecules (50) to the simulation box and, after an energy minimization, continued running at 1400 K with the peptide still restrained. The root mean square displacement of lipid molecules over 2 ns was approximately 8.5 nm. During this run, we harvested four configurations, one every 2 ns, that served as independent starting configurations for separate realizations of the self-assembly process, which we label as A, B, C and D. This procedure for obtaining four independent configurations was carried out for each variant of the peptide (GAD-1, GAD-1p, GAD-2 and GAD-2p) as well as for a system without a peptide, which acts as a control. In total, there were starting points for 20 simulations of the self-assembly process.

Each self-assembly simulation began with a brief simulation of 100 ps under conditions of constant temperature and constant pressure, with the peptide unrestrained. The temperature was held constant at 310 K with the Nose–Hoover algorithm and a time constant of 0.1 ps. An isotropic pressure of 1 bar was maintained with the Parrinello–Rahman algorithm employing a time constant of 5 ps and compressibility of 4.5×10^{-5} bar^{-1}. This short simulation was sufficiently long to bring the density into a steady state (it does not continue to evolve in

Table 1
Parameters and measurement summary for each simulation. The calculations for bilayer width, pore diameter (P) and pore diameter (W) were done for last 100 ns of simulations. A, B, C and D represent individual runs of the same system composition.

System	Number of atoms	Time (ns)	Class type	Bilayer width (nm)	Pore diameter (P) (nm)	Pore diameter (W) (nm)
POPC-A	36,368	400.00	–	4.24 ± 0.09	0.69 ± 0.16	1.08 ± 0.13
POPC-B	36,368	400.00	–	4.22 ± 0.09	0.66 ± 0.16	1.05 ± 0.13
POPC-C	36,368	400.00	–	4.27 ± 0.09	0.52 ± 0.18	0.98 ± 0.14
POPC-D	36,368	400.00	–	4.26 ± 0.08	0.71 ± 0.18	1.09 ± 0.13
GAD-1-A	36,728	376.00	1	4.25 ± 0.09	0.47 ± 0.17	0.98 ± 0.18
GAD-1-B	36,728	370.40	1	4.15 ± 0.10	0.53 ± 0.18	1.03 ± 0.14
GAD-1-C	36,728	348.00	5	4.31 ± 0.09	0.59 ± 0.16	1.00 ± 0.12
GAD-1-D	36,728	344.00	2	4.21 ± 0.08	0.37 ± 0.15	0.92 ± 0.23
GAD-1p-A	36,498	344.00	1	4.17 ± 0.08	0.62 ± 0.21	1.18 ± 0.21
GAD-1p-B	36,498	320.00	1	4.22 ± 0.08	0.82 ± 0.14	1.14 ± 0.11
GAD-1p-C	36,498	328.00	4	4.28 ± 0.09	0.81 ± 0.16	1.13 ± 0.11
GAD-1p-D	36,498	304.00	1	4.24 ± 0.09	0.57 ± 0.17	1.01 ± 0.16
GAD-2-A	36,576	336.00	3	4.01 ± 0.08	–	–
GAD-2-B	36,576	332.00	2	4.25 ± 0.09	0.77 ± 0.21	1.18 ± 0.10
GAD-2-C	36,576	335.60	2	4.25 ± 0.09	0.52 ± 0.20	1.15 ± 0.13
GAD-2-D	36,576	324.00	2	4.19 ± 0.08	0.40 ± 0.20	1.04 ± 0.17
GAD-2p-A	36,624	323.60	3	4.22 ± 0.09	0.74 ± 0.18	1.10 ± 0.13
GAD-2p-B	36,624	332.00	2	4.26 ± 0.09	0.79 ± 0.12	1.21 ± 0.13
GAD-2p-C	36,624	348.00	4	4.24 ± 0.10	0.64 ± 0.16	1.01 ± 0.13
GAD-2p-D	36,624	328.00	1	4.21 ± 0.09	0.58 ± 0.16	1.06 ± 0.15

subsequent steps), as well as to allow the large fluctuations expected after a large drop in temperature to subside. This run was short enough so that no significant change in the helicity of the peptide occurred and the lipid molecules did not show any appreciable progress towards bilayer assembly. The final box size was roughly 7.25 nm on each side.

At this point we began the "production" run (Fig. 2), using a time step of 2 fs and a radial cutoff of 1.2 nm for the real space force calculations. We used the particle mesh Ewald method for Columbic interactions with a Fourier spacing of 0.15 nm and interpolation order of four (cubic). The temperature and pressure controls were as for the previous step, with the exception that we use anisotropic pressure scaling in order to avoid enforcing a bilayer normal direction. The average run time for these production simulations was approximately 350 ns (Table 1). The beginning of these runs marks our time origin ($t = 0$).

We note that in some of our runs, anisotropic scaling allowed for one of the dimensions of the box to shrink below the potential cutoff, effectively ending the simulation. In retrospect, we could have used anisotropic rescaling until the bilayer had formed, and then switched to semi-isotropic scaling to avoid this problem. In reality, we generated additional starting configurations so as to have four realizations of each variant and to maintain a uniform protocol across runs.

To characterize the evolution and structure of our systems, we tracked the potential energy of the system, lipid acyl-chain order parameter (as defined in Salgado et al. (38)), the width of lipid bilayer, pore size, secondary structure of the peptide, mean square displacement of particles and the number of water molecules around different peptide residues. To find the mean value of order parameter of acyl-chains as a function of time, for each frame we calculated the order parameter of each of the carbons in the unsaturated acyl-chain and averaged over all of these carbons. The utilities included with GROMACS, such as g_energy, g_density, g_order, g_msd and g_rdf, as well as the Define Secondary Structure of Proteins (DSSP) (51,52) plugin of the Visual Molecular Dynamics (VMD) software package (53,54) were used to obtain these quantities.

To determine the pore size, we first needed to determine the location of the pore axis. To do this, we found all interior P atoms, i.e., those residing within 1.5 nm of the midway plane between bilayer leaflets. (We defined the location of a leaflet along the bilayer normal

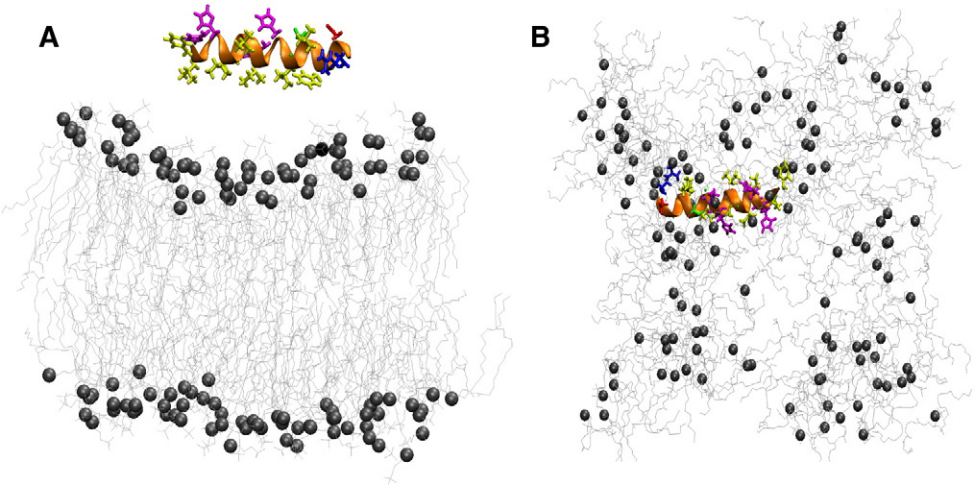

Fig. 1. System setup. The peptide was initially configured as a canonical helix and placed in the simulation box with an assembled POPC lipid bilayer (A). Keeping the peptide position restrained, the molecule positions were randomized by heating the system to 1400 K for 2 ns (B). The peptide backbone is shown as an orange ribbon, the histidine sidechains in purple, hydrophobic sidechains in yellow, polar uncharged sidechains in green, positively charged sidechains in blue, and negatively charged sidechains in red. The gray spheres represent the lipid headgroup phosphorus atoms and the silver lines, the lipid acyl-chains.

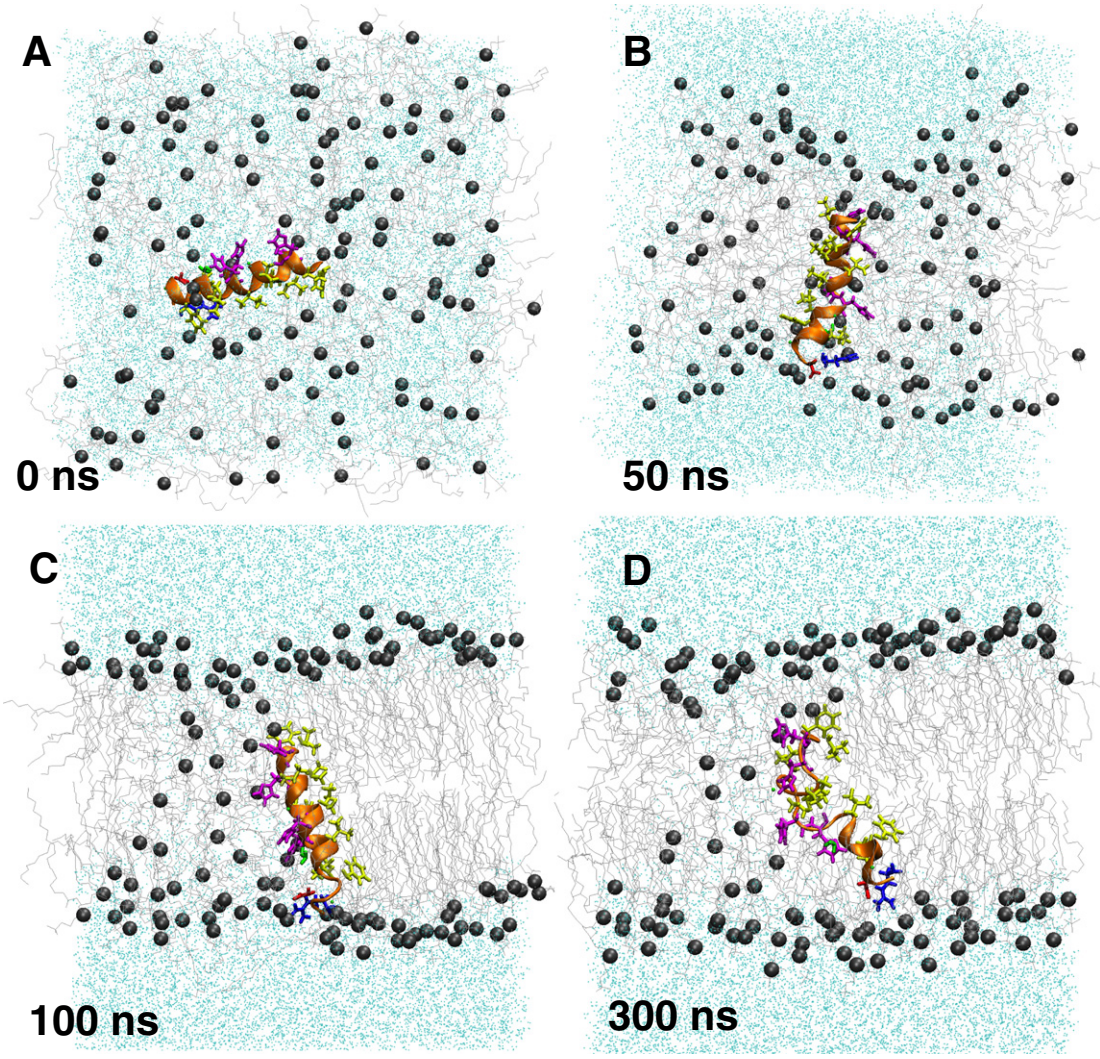

Fig. 2. Representative snapshots of the molecular dynamics simulation of GAD-2 peptide realization set C in POPC. (A) At the start of the production run (0 ns) with randomized lipid positions. (B) After 50 ns, a more ordered, bilayer-like configuration is observed. (C) The peptide is positioned inside a bilayer (100 ns). Although the bilayer appears ordered with sharply defined lipid head group positions, a pore is present. (D) After 300 ns, the bilayer still has a pore and the peptide is found inside the bilayer, proximal to the pore. The peptide backbone is shown as an orange ribbon, the histidine sidechains in purple, hydrophobic sidechains in yellow, polar uncharged sidechains in green, positively charged sidechains in blue, and negatively charged sidechains in red. The gray spheres represent the lipid headgroup phosphorus atoms, the silver lines represent the lipid acyl-chains, and water is shown as cyan dots.

as a peak in the P density profile). On average, for a given simulation frame, there are six such interior P atoms. The pore axis, which by definition is parallel to the bilayer normal, passes through the center of mass of the interior P atoms and was defined on a frame-by-frame basis. The radius of the pore, by one definition, was the average perpendicular distance of the interior P atoms to the axis. Alternatively, we defined the pore size by considering all distances between the interior water molecules (defined in the same way as interior P atoms), and finding the largest perpendicular distance. Since there was the occasional water molecule that diffused deep into the bilayer, in calculating the average pore size, we discarded the largest 5% of sizes. We determined this cutoff by looking at the distribution of pore sizes.

To calculate the percentage of time each peptide residue takes on a helical structure we used VMD software (version 1.9.1). We found the secondary structure of each residue frame-by-frame in VMD, and then used this to calculate the percent helicity per residue during the last 100 ns of the simulation (except for GAD-1p-A, where the last 70 ns was used). Both alpha-helical and 3–10 helical structures were used to generate the percent helical structure.

3. Results

3.1. Peptide-free systems

We first investigated the behavior of the POPC/water systems in the absence of peptide (POPC-A, POPC-B, POPC-C, POPC-D in Table 1). After starting with the lipids in randomized positions, all four simulations reach apparent equilibrium after ~100 ns, as judged by multiple parameters, including potential energy and the mean value of order parameter of the lipid chains (Fig. 3). From ~100 ns to the end of the simulations at ~400 ns, all 4 systems display a bilayer with a single pore. The pore consists of a contiguous water-containing hole through both leaflets of the bilayer that is lined by phospholipid headgroups. The area per headgroup of the lipids lining the pores is larger than the area per headgroup for lipids found in the planar region of the bilayer.

The bilayer width was found to be between 4.2 and 4.3 nm (Table 1) as defined by the distance between the phosphorous atoms in the lipid head groups. The sizes of the pores varied from simulation to simulation, but were in the range of 1.0 to 1.1 nm when measured using

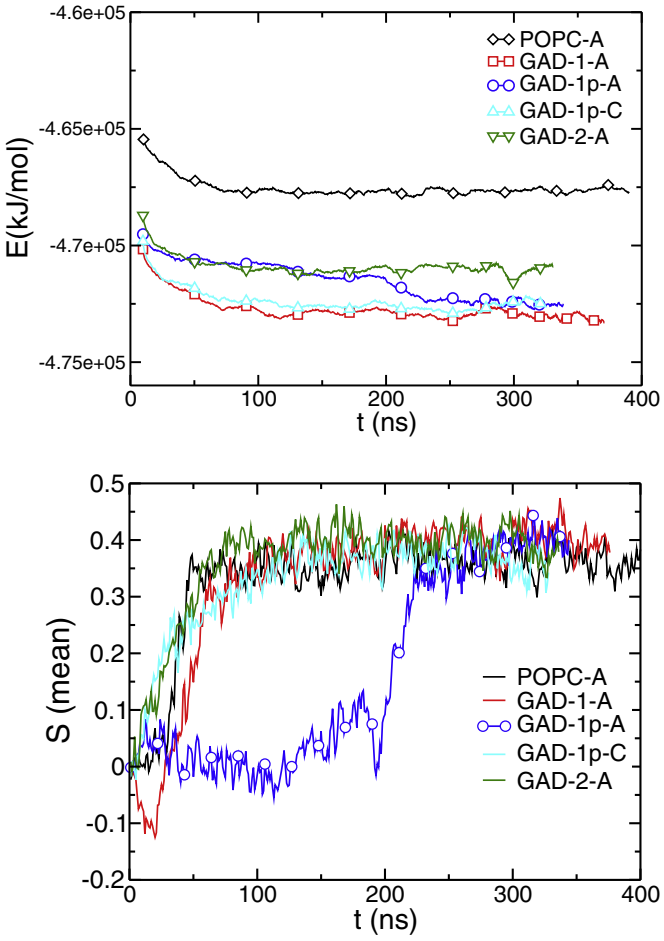

Fig. 3. Time evolution of potential energy (top) of the system and mean value of the order parameter of the acyl-chain (bottom) during representative simulations. In the top panel, shown are running averages over 50 data points, with 400 ps between data points.

water, and in the range of 0.5 nm to 0.8 nm when measured using phosphorous (Table 1). The difference in pore size for the two measurements illustrates that water penetrates well into the lipids of the pore. As we shall discuss, this more aqueous environment plays an important role in understanding the structure and positioning of the peptide near the pore.

3.2. Systems with peptides

Next, we added peptide to our systems. We studied four peptides, GAD-1, GAD-1p, GAD-2, and GAD-2p, where "p" denotes the form of the peptide with histidines positively charged. Each peptide was subjected to four independent simulations A, B, C and D (Table 1). Initially, during randomization, the peptides started in a canonical helical structure but were subsequently simulated at ambient conditions without restraints (Fig. 2).

Similar to the lipid-only simulations, 15 out of 16 of the peptide–lipid simulations reach apparent equilibrium after ~100 ns. There was one outlier; the GAD-1p-A system took ~230 ns to generate the bilayer (Fig. 3). The GAD-1p-A system initially formed with two separate micelles, which eventually coalesced into one micelle and then formed the bilayer. All but one of the peptide-containing systems formed pores (Fig. 4). The one exception was GAD-2-A, the only simulation with a perfect bilayer without a pore (Fig. 4C).

As for the systems without peptide, the sizes of the pores varied from simulation to simulation, but were in the range of 1.0 to 1.2 nm when measured using water and in the range of 0.5 nm to 0.8 nm when measured using phosphorous (Table 1). These are similar to pore sizes in the systems without peptide. The bilayer width, defined by the distance between the phosphorous atoms in the head groups, is between 4.0 and 4.3 nm, i.e. also in the same range as for systems without peptide. Thus, the peptide does not appear to have any large effect on the pore size or bilayer width.

As detailed below, in most cases (13 out of 15), the peptide preferentially interacts with the pore, rather than with the planar region of the bilayer. One reason for this preference may be the decreased density of lipid head groups in the pore (~0.8 nm^{-2}) as compared to the planar region (~1.5 nm^{-2}). The reduced head group density in the pore may allow the peptide enough space to position in such a way so as to interact optimally with both the hydrophobic region of the lipids and the hydrophilic headgroup/water region.

3.3. Peptide structure and residue hydrophobic/hydrophilic partitioning

During the self-assembly process, there were no restraints on the peptide, allowing its structure to evolve freely as the bilayer formed. Following apparent equilibrium at ~100 ns, the structure of each peptide continued to evolve, but did not change significantly in the last 100 ns. When compared to each other, the final structures of the peptides exhibit substantial heterogeneity i.e., even for different independent simulations of the same peptide, there are different degrees of overall helicity and variations in the regions that are helical (Fig. 5). Despite the structural heterogeneity, the partitioning of each residue into either a hydrophobic or hydrophilic environment is very similar. Specifically, the number of water molecules within a set distance of the center of mass of each residue (Fig. 6) is quite consistent across the 4 different independent simulations of each system. The observed structural heterogeneity is expected and is consistent with both experiments on membrane-active peptides (55) and simulations of AMPs (39,56). There is no apparent difference between how the peptides with protonated histidines versus those with neutral histidines behave in terms of helicity and proximity to water.

3.4. Peptide-pore interactions

Of the 15 out of 16 peptide simulations that form a pore, 14 of these show the peptide interacting closely with the pore. This is evident from Fig. 7, where all but one of the peptides (GAD-2p-A) has at least one residue with its center of mass within 0.7 nm of the pore (represented by the dotted lines).

The systems can be classified into five different types, depending on the mode of interaction between the peptide and the pore in the last 100 ns of each simulation. In the first and most common type (6/16 systems), there are extensive interactions between the pore and one of the terminal halves of the peptide, while the other half of the peptide remains relatively distal from the pore and in the planar region of the bilayer (Fig. 4A). The region of the peptide that interacts closely with the pore takes on an oblique angle with respect to the plane of the membrane, while the non-interacting peptide half positions more nearly parallel to the membrane surface. The second most common type of system (5/16 systems) is exemplified in Fig. 4B, where the entire peptide is proximal to the pore and makes extensive interactions with lipids from both leaflets of the bilayer. In the third type of system (2/16), the peptide interacts with the planar region of one of the bilayer leaflets without interacting with a pore, e.g. Fig. 4C and Fig. 4D. The fourth class (2/16) consists of systems (GAD-1p-C and GAD-2p-C) in which just one residue in the peptide (H3) interacts with the rim of the pore and the rest of the peptide is not in contact with the pore, but positions within the nearest leaflet, Fig. 4E. The remaining simulation, GAD-1-C, does not fit within any of these 4 schemes and thus is the sole occupant of the Class 5 type of system. Here, the peptide embeds deeply in the bilayer, but with a position nearly parallel to the bilayer surface.

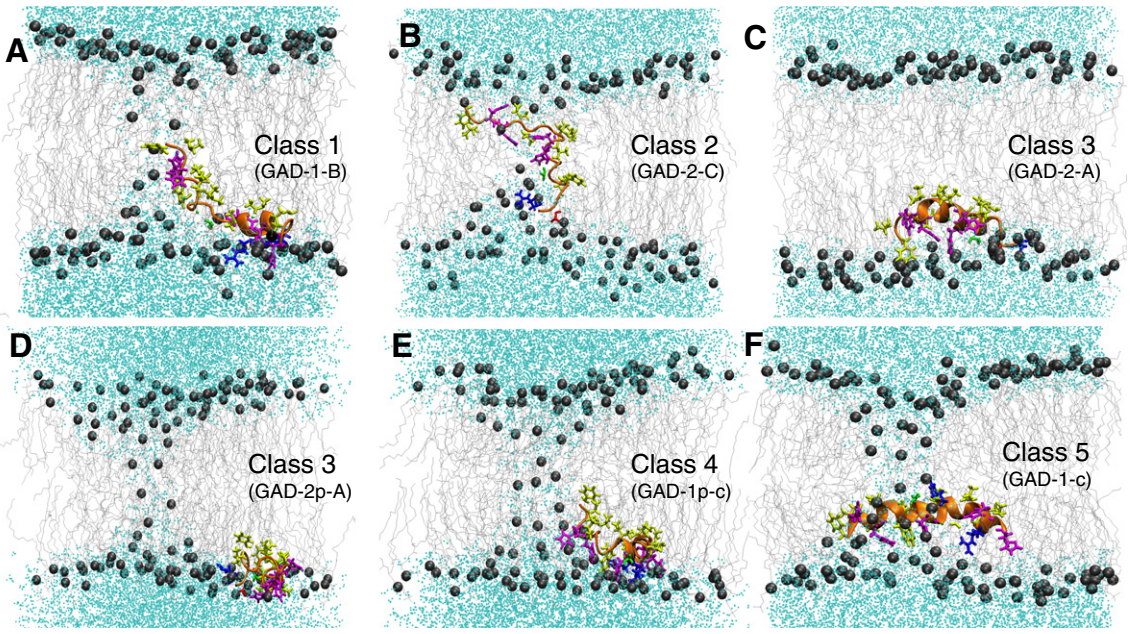

Fig. 4. (A–F): Selected snapshots from near the end (~350–400 ns) of the simulations. The peptides exhibit a variety of final structures and topologies within the bilayer, but the systems can be grouped into five types of configurations as described in the text and labeled on the panels. The peptide backbone is shown as an orange ribbon, the histidine sidechains in purple, hydrophobic sidechains in yellow, polar uncharged sidechains in green, positively charged sidechains in blue, and negatively charged sidechains in red. The gray spheres represent the lipid headgroup phosphorus atoms, and the silver lines, the lipid acyl-chains. Water molecules are in cyan.

It appears that, at least on the timescale of these simulations, there is no inter-conversion between class types during the simulation for class 1 and class 2 systems. On the other hand, there were two observed cases where systems started out as class 3 type – i.e. peptide not interacting with the pore – converting to a class 4 type – peptide interacting with the rim of the pore – during the course of the simulation.

The four different peptides, GAD-1, GAD-1p, GAD-2, and GAD-2p show different propensities to form these five types of systems. GAD-1 and GAD-1p both showed a strong tendency to display class 1 configurations, where one end of the peptide interacts with the pore, and the other end interacts with the planar region of one bilayer leaflet (Fig. 4A). One of the exceptions to this trend was also interesting; GAD-1-C is a unique configuration among the 16 peptide-containing

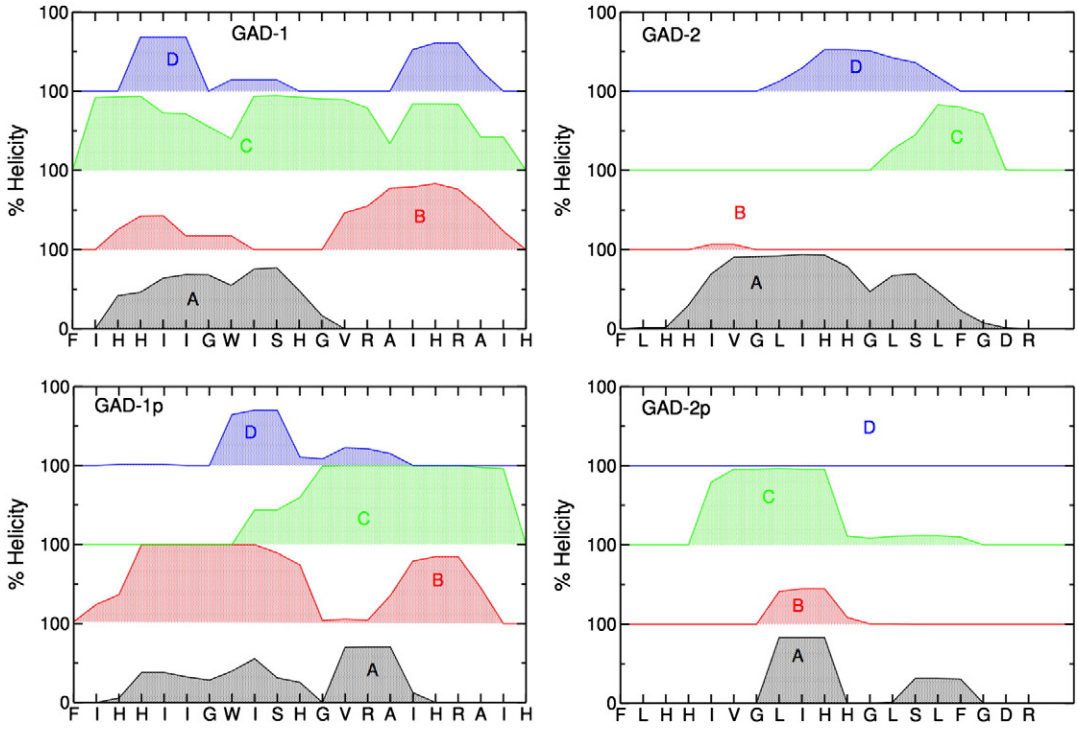

Fig. 5. Percentage of helical structuring of GAD peptides during last 100 ns of simulation (except GAD-1p-A which is for the last 70 ns). A, B, C and D represent individual runs of the same system composition.

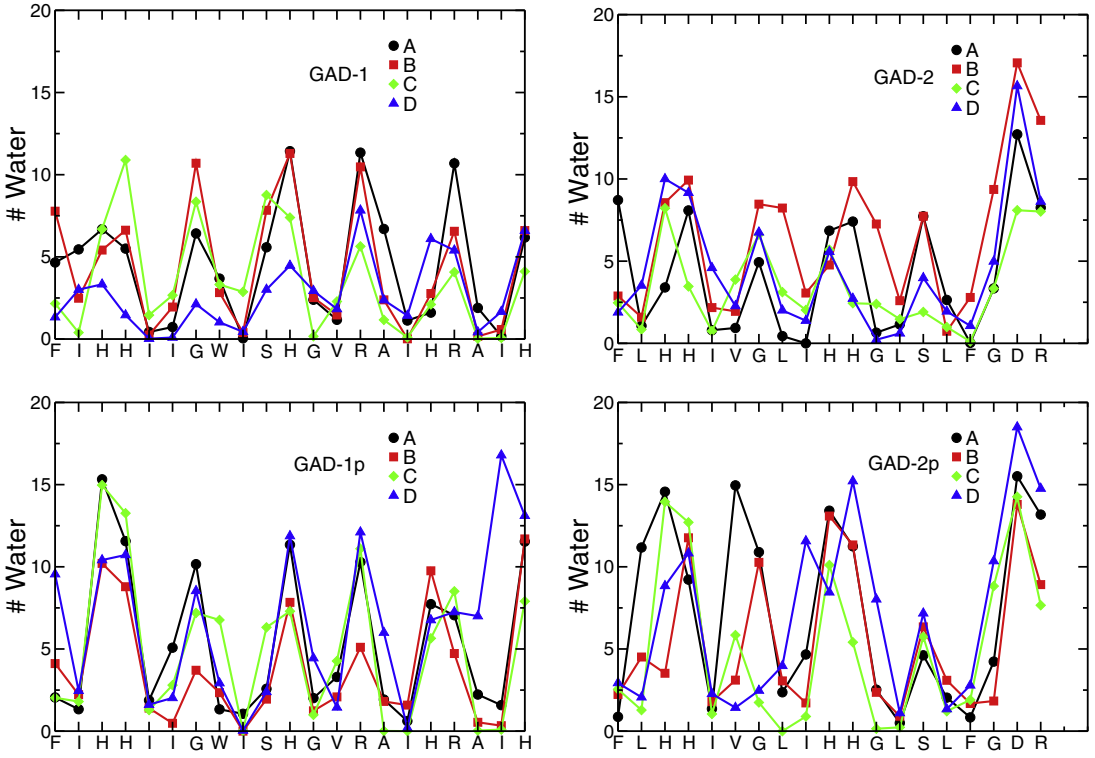

Fig. 6. Number of water molecules within r = 0.65 nm of the center of mass of each GAD residue in the last 100 ns of simulation (except GAD-1p-A which is for the last 70 ns). A, B, C and D represent individual runs of the same system composition.

systems (Fig. 4F) with the peptide located in proximity to the pore, deeply embedded in the bilayer with a position parallel to the bilayer normal. Intriguingly, this system has the highest helical structure among all simulations.

In contrast to GAD-1 and GAD-1p, the GAD-2 systems are in class two configurations, with the exception of GAD-2-A. In the GAD-2-A system there is no pore. Notably, GAD-2-A also has the most helical structure among GAD-2 simulations. As explored in the Discussion section, it

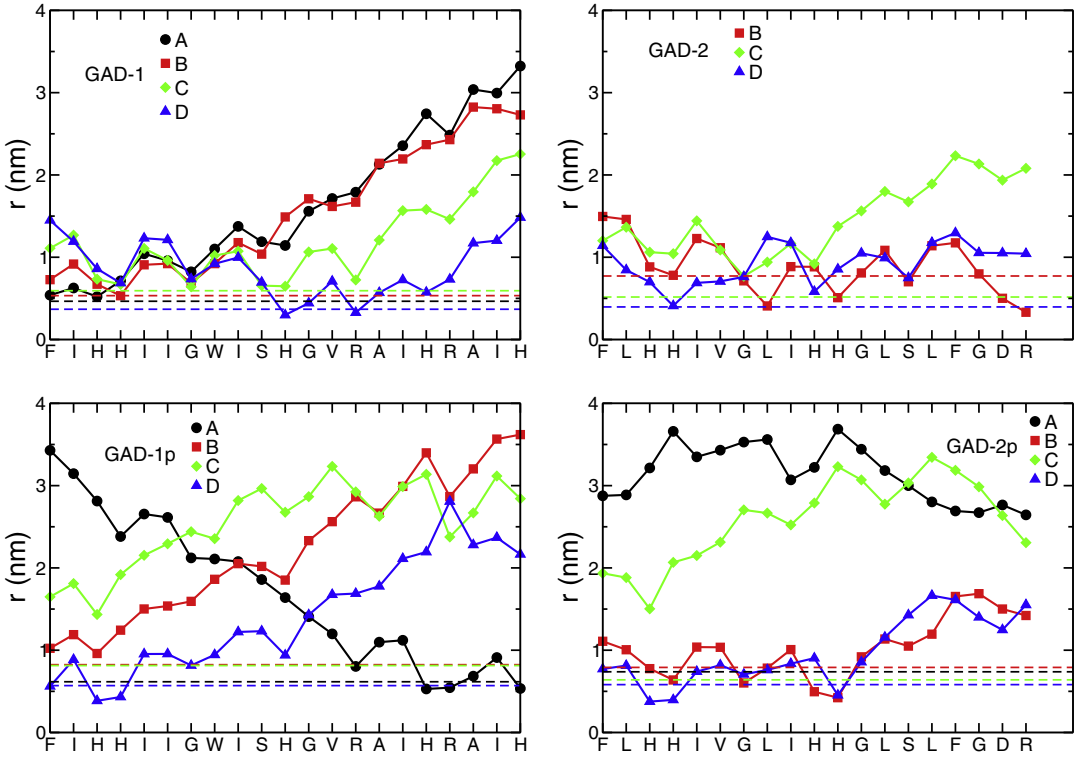

Fig. 7. The distance of the center of mass of each residue from the central axis of the pore (lines and symbols) and the radius of pore (dotted lines), as defined by lipid phosphorous position during last 100 ns (except GAD-1p-A which is for last 70 ns) of simulation. A, B, C and D represent individual runs of the same system composition.

may well be significant that the two most helical peptides, GAD-1-C and GAD-2-A, also display the most parallel orientation with respect to the bilayer surface. The GAD-2p sets of simulations are the most heterogeneous in terms of the observed topology and we observe four different types of systems (Table 1).

3.5. Role of histidine pairs in AMP-pore interactions

One notable observation is that the N-terminal half of all 4 peptides has a greater tendency to interact with the pore than the C-terminal half (Fig. 7). Again the exceptional case is GAD-1p-A, in which the C-terminal half interacts with the pore. A potential explanation for the strong preference for the N-terminal half to interact with the pore is the pair of histidines, (H3 and H4) that are located near the N-terminal half of both peptides. Consistent with this explanation, the 2nd pair of histidines (H10 and H11) present only in GAD-2, are also found consistently in close proximity to the pore (Fig. 7). It appears that there is no need for the histidine pair to be charged in order to interact closely with the POPC pore; even uncharged histidine pairs exhibit this behavior.

To assess the importance of the pairing of the histidines to pore interactions, we can compare the behavior of the H3–H4 pair to the only other charged pair of amino acids in the peptides, the H17 and R18 present in GAD-1p. The H17–R18 pair has a markedly lower tendency to interact with the pore compared to either the H3–H4 motif present in both peptides or the H10–H11 motif present in the GAD-2 peptides (Fig. 7). Specifically, 7 out of 8 of the GAD-1/1p systems show much closer interactions between the pore and the H3–H4-containing N-terminal region of the peptide compared to the H17–R18-containing C-terminal region of the protein.

A potential alternate explanation for the behavior of the histidine pairs is that the pore-interaction behavior might originate not from the histidines, but from their neighboring residues. However, this does not appear to be the case as the residues adjacent to the H3–H4, H10–H11 and H17–R18 pairs are all hydrophobic.

4. Discussion

In this work, we employ an approach to molecular dynamics simulation that allows the bilayer to self-assemble (38). This has the advantage of preventing bias, but also prevents us from observing the early kinetic step in which the peptide binds the bilayer and begins to translocate. To be clear, in our system set-up, pores are formed even in the absence of peptide, and therefore our studies indicate details of peptide/bilayer interactions, rather than the kinetic process of peptide-induced pore formation. None-the-less, in combination with multiple independent simulations of each system composition, this approach has the advantage of illustrating the variety of peptide/lipid structures with favorably low energy. The final peptide structures observed exhibit a wide variety of helicity (Fig. 5), but a high degree of conservation of peptide–lipid interactions at the individual amino acid level (Fig. 6). The simulations thus provide atomic-level insight into the structural plasticity that has long been observed experimentally for many helical AMPs and has been argued to be a key part of their potency and selectivity (55,57). The observed structural heterogeneity relates to the concept of "imperfect amphipathicity" which suggests that AMP structures that present a few polar/charged residues on a non-polar face promote the formation/stabilization of pores (58,59). In keeping with these ideas around AMP structural heterogeneity and imperfect amphipathicity, we observed that the most helical and perfectly amphipathic peptide structures (GAD-1-C and GAD-2-A) position parallel to the bilayer surface and tend to interact with the planar part of the bilayers formed. On the other hand, the majority of the simulations showed peptides with smaller helical contents interacting with the curved region of the bilayer in the pore. A variety of models have been employed in trying to understand AMP-induced pore formation, including the toroidal pore, carpet and barrel-stave models (3), and the two-state model (60), but the results with the Gad peptides are probably better understood in the context of models that capture the polymorphic/disordered characteristics of many AMPs, such as Bechinger et al. (55) and Sengupta et al. (56).

Another advantage of the self-assembly method is the appearance of a pore when the bilayer first forms. This allows us to determine whether and how the peptide interacts with a pore. The long lifetime of the pore, present even in the lipid-only simulations, is thus beneficial. While this persistence of the pore in our system is not unexpected, as explained by Fuertes et al. (61), it is significantly longer than the mere tens of nanoseconds reported in previous self-assembly studies (38,62). Repeating our self-assembly protocol for the lipid-only system with the SPC model of water, which was used in previous studies, instead of TIP4P, which we used in this work, we observed significantly faster bilayer formation and a pore lifetime of 50 ns. This consistency with previous work indicates that the choice of water model can have a significant effect on membrane dynamics. This is not surprising given that seemingly small differences between water models can yield significantly different thermodynamic properties of simulated water (63). We did examine other possible sources for this discrepancy including temperature, pressure control and other protocol details, and found no significant changes. Extending one of our lipid-only simulations (with TIP4P) reveals that the pore persists to at least 1 μs, and that the membrane is rather fluid, given a root-mean-square displacement of P atoms of approximately 2 nm in 100 ns. This confirms the view that the membrane-with-pore is a well-defined metastable state quite stable to thermal fluctuations, rather than a kinetically hindered state slowly and continuously moving towards equilibrium.

More specifically to histidine-containing AMPs, we observed a marked preference for the N-terminal half of GAD-1 and GAD-2 to interact more closely with the pore than the C-terminal half of the peptides (Fig. 7). This preference corresponds well to the location of the sequential pairs of histidines, which are themselves much more closely positioned to the pores compared to other types of charged pairs such as histidine-arginine. There are substantial differences in structure between histidine and arginine (or lysine) sidechains that might underlie the apparent differences in lipid interactions. Histidine represents a relatively compact, constrained sidechain that, due to the two nitrogens present in the ring, has a hydrophilic nature in both its charged and uncharged states. On the other hand, arginine consists of a long, conformationally flexible hydrophobic chain with a positively charged moiety at the terminus — and is thus most precisely viewed as amphipathic in character. Arginine has a well-known propensity to "snorkel" (64,65) i.e. embed its hydrophobic region in acyl chains of the bilayer and extend the charged terminal group out to the polar head group region. In comparison, a histidine–histidine pair presents a relatively conformationally constrained hydrophilic moiety that may not be able to interact easily with the densely packed lipid headgroups in the planar part of the bilayer. By contrast, the lipid headgroups in the pore are less tightly packed together and there is also more water available for favorable hydrophilic interactions and may thus provide a more energetically favorable site for the histidine pair to interact.

This potential explanation is consistent with the observation that even the uncharged histidine pairs associate with the pores and is interesting to consider in the light of studies which suggest that some histidine-containing AMPs have increased selectivity, even at neutral pH (22). For example, Ruangsri et al have probed the antimicrobial activity of peptides with almost identical sequences to GAD-1 and GAD-2 and suggested that while the GAD-1-like peptide has broad spectrum antimicrobial activity, the GAD-2-like peptide seems to be much more specific and was only found to be active against the fish parasite, *Tetrahymena pyriformis* (26). It is possible that the inclusion of histidine-pairs, perhaps in combination with the reduction in overall positive charge at neutral pH as in GAD-2 compared to GAD-1, presents one

mechanism by which evolution may "tune" the structure–activity relationships of AMPs for specificity against particular types of pathogens. Note that, our observed absence of alteration in histidine–lipid interactions when histidine's charge is modified does not preclude a role for histidine charge in selectivity. It may well be the case that the more charged versions of the peptides bind more strongly to certain membranes, in particular to anionic ones, thus effecting membrane selectivity without necessarily affecting the mode of lipid interaction once it is bound.

In a final thought on the differences between GAD-1 and GAD-2, Fig. 8 schematically represents the two paralogs and the way they tend to interact with a pore in the bilayer. The H–H pairs prefer the more highly curved, central region of the pore where the increased spacing between head groups allows the compact, conformationally constrained pair of sidechains to interact favorably at the interface. On the other hand, the H–R pair is more able to interact with the more ordered, planar region. The basic premise of our simulations is that the structures we observe are representative of low free energy configurations and thus the differences in preferred positions suggest potentially interesting differences in the kinetics of how the pores are formed i.e., the GAD-1 preferred mode of interaction is suggestive of a more easily accessible initial defect-promoting step, whereas the GAD-2 preferred configuration is achieved more easily in the presence of a complete pore. The heterogeneity in the final structures observed in our simulations suggests a kind of "stroboscopic" view of the potential kinetics of peptide promoted pore formation, with an initial interaction of the peptide with a planar bilayer looking like Fig. 4C, followed by the promotion of a defect in one leaflet as in Fig. 4E and then Fig. 4A, and perhaps translocation across the pore as in Fig. 4B.

The model suggested by these simulations will be useful in the interpretation of experimental solution and solid-state NMR studies of Gad-1 and Gad-2 currently being performed in our lab. Another interesting issue to be addressed is the role of peptide oligomerization in pore interactions, as many AMPs are thought to form dimers, or higher order oligomers in order to exhibit their maximum toxicity (66–68). Further studies employing more than one GAD peptide in the simulation box would help address this question.

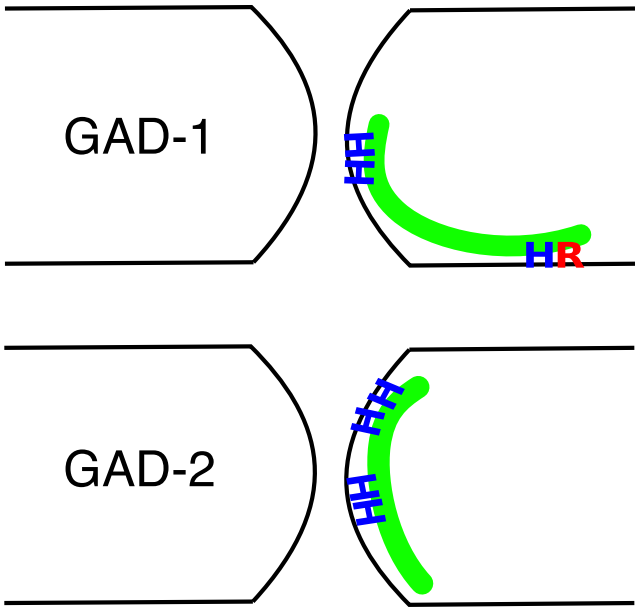

Fig. 8. Schematic figure showing the two most favorable positions of GAD-1 and GAD-2 peptides.

Acknowledgements

We are grateful to Michael Morrow and Anand Yethiraj for the insightful discussions. Computational facilities were provided by ACEnet, the regional high performance computing consortium for universities in Atlantic Canada. ACEnet is funded by the Canada Foundation for Innovation (CFI), the Atlantic Canada Opportunities Agency (ACOA), and the provinces of Newfoundland and Labrador, Nova Scotia, and New Brunswick. We acknowledge NSERC for the partial funding. MHK received support through an ACEnet Graduate Fellowship and MB received support through an ACEnet/SUN Microsystems Postdoctoral Research Fellowship.

References

[1] G. Wang, X. Li, Z. Wang, Nucleic Acids Res 37 (2009) D933–D937.
[2] M. Zasloff, Nature 415 (2002) 389–395.
[3] K.A. Brogden, Nature Reviews Microbiology 3 (2005) 238–250.
[4] L.T. Nguyen, E.F. Haney, H.J. Vogel, Trends Biotechnol 29 (2011) 464–472.
[5] B. Bechinger, E.S. Salnikov, Chem Phys Lipids 165 (2012) 282–301.
[6] M.D. Seo, H.S. Won, J.H. Kim, T. Mishig-Ochir, B.J. Lee, Molecules 17 (2012) 12276–12286.
[7] A.T. Yeung, S.L. Gellatly, R.E. Hancock, Cell Mol Life Sci 68 (2011) 2161–2176.
[8] L.M. Rossi, P. Rangasamy, J. Zhang, X.Q. Qiu, G.Y. Wu, J Pharm Sci 97 (2008) 1060–1070.
[9] D.W. Hoskin, A. Ramamoorthy, Biochim Biophys Acta 1778 (2008) 357–375.
[10] S. Al-Benna, Y. Shai, F. Jacobsen, L. Steinstraesser, Int J Mol Sci 12 (2011) 8027–8051.
[11] C. Yates, S. Sharp, J. Jones, D. Topps, M. Coleman, R. Aneja, J. Jaynes, T. Turner, Biochem Pharmacol 81 (2011) 104–110.
[12] P. Grieco, V. Luca, L. Auriemma, A. Carotenuto, M.R. Saviello, P. Campiglia, D. Barra, E. Novellino, M.L. Mangoni, J Pept Sci 17 (2011) 358–365.
[13] N. Papo, Y. Shai, Biochemistry 42 (2003) 9346–9354.
[14] L. Steinstraesser, J. Hauk, C. Schubert, S. Al-Benna, I. Stricker, H. Hatt, Y. Shai, H.U. Steinau, F. Jacobsen, PLoS One 6 (2011) e18321.
[15] R. Rathinakumar, W.C. Wimley, FASEB J 24 (2010) 3232–3238.
[16] L. Kacprzyk, V. Rydengard, M. Morgelin, M. Davoudi, M. Pasupuleti, M. Malmsten, A. Schmidtchen, Biochim Biophys Acta 1768 (2007) 2667–2680.
[17] A. Makovitzki, A. Fink, Y. Shai, Cancer Res 69 (2009) 3458–3463.
[18] I.H. Lee, Y. Cho, R.I. Lehrer, Infection and immunity 65 (1997) 2898–2903.
[19] Z. Tu, A. Young, C. Murphy, J.F. Liang, J Pept Sci 15 (2009) 790–795.
[20] K. Chikakane, H. Takahashi, Clinics in dermatology 13 (1995) 299–306.
[21] I.F. Tannock, D. Rotin, Cancer research 49 (1989) 4373–4384.
[22] R. Kharidia, Z. Tu, L. Chen, J.F. Liang, Arch Microbiol 194 (2012) 769–778.
[23] J. Georgescu, V.H. Munhoz, B. Bechinger, Biophys J 99 (2010) 2507–2515.
[24] M.J. Browne, C.Y. Feng, V. Booth, M.L. Rise, Dev Comp Immunol 35 (2011) 399–408.
[25] J. Ruangsri, J.M.O. Fernandes, J.H.W.M. Rombout, M.F. Brinchmann, V. Kiron, BMC veterinary research 8 (2012) 46.
[26] J. Ruangsri, S.A. Salger, C. Caipang, V. Kiron, J.M.O. Fernandes, Fish & Shellfish Immunology 32 (2012) 396–406.
[27] J.M.O. Fernandes, J. Ruangsri, V. Kiron, Plos one 5 (2010) e9501.
[28] S. Campagna, N. Saint, G. Molle, A. Aumelas, Biochemistry 46 (2007) 1771–1778.
[29] E.Y. Chekmenev, S.M. Jones, Y.N. Nikolayeva, B.S. Vollmar, T.J. Wagner, P.L. Gor'kov, W.W. Brey, M.N. Manion, K.C. Daugherty, M. Cotten, J Am Chem Soc 128 (2006) 5308–5309.
[30] E.Y. Chekmenev, B.S. Vollmar, K.T. Forseth, M.N. Manion, S.M. Jones, T.J. Wagner, R.M. Endicott, B.P. Kyriss, L.M. Homem, M. Pate, J. He, J. Raines, P.L. Gor'kov, W.W. Brey, D.J. Mitchell, A.J. Auman, M.J. Ellard-Ivey, J. Blazyk, M. Cotten, Biochim Biophys Acta 1758 (2006) 1359–1372.
[31] A.A. De Angelis, C.V. Grant, M.K. Baxter, J.A. McGavin, S.J. Opella, M.L. Cotten, Biophys J 101 (2011) 1086–1094.
[32] R. Fu, E.D. Gordon, D.J. Hibbard, M. Cotten, J Am Chem Soc 131 (2009) 10830–10831.
[33] S.A. Lee, Y.K. Kim, S.S. Lim, W.L. Zhu, H. Ko, S.Y. Shin, K.S. Hahm, Y. Kim, Biochemistry 46 (2007) 3653–3663.
[34] H.J. Lin, T.C. Huang, S. Muthusamy, J.F. Lee, Y.F. Duann, C.H. Lin, Zoolog Sci 29 (2012) 327–332.
[35] F. Mehrnejad, M. Zarei, J Biomol Struct Dyn 27 (2010) 551–560.
[36] S.F. Niu, Y. Jin, X. Xu, Y. Qiao, Y. Wu, Y. Mao, Y.Q. Su, J. Wang, Fish Shellfish Immunol 35 (2013) 513–524.
[37] T. Yuan, X. Zhang, Z. Hu, F. Wang, M. Lei, Biopolymers 97 (2012) 998–1009.
[38] S. Esteban-Martín, J. Salgado, Biophysical journal 92 (2007) 903–912.
[39] H. Leontiadou, A.E. Mark, S.J. Marrink, J Am Chem Soc 128 (2006) 12156–12161.
[40] J.P. Ulmschneider, J.P.F. Doux, J.A. Killian, J.C. Smith, M.B. Ulmschneider, J. Chem. Theory Comput. 5 (2009) 2202–2205.
[41] K. Arnold, L. Bordoli, J. Kopp, T. Schwede, Bioinformatics 22 (2006) 195–201.
[42] F. Kiefer, K. Arnold, M. Kunzli, L. Bordoli, T. Schwede, Nucleic Acids Res 37 (2009) D387–D392.
[43] M.C. Peitsch, Bio-Technology 13 (1995) 658–660.
[44] http://www.expasy.org/spdbv/ .
[45] W. Zhao, T. Rog, A.A. Gurtovenko, I. Vattulainen, M. Karttunen, Biophys J 92 (2007) 1114–1124.
[46] S. Pronk, S. Páll, R. Schulz, P. Larsson, P. Bjelkmar, R. Apostolov, M.R. Shirts, J.C. Smith, P.M. Kasson, D. van der Spoel, Bioinformatics 29 (2013) 845–854.

[47] W.L. Jorgensen, D.S. Maxwell, J. Tirado-Rives, Journal of the American Chemical Society 118 (1996) 11225–11236.
[48] G.A. Kaminski, R.A. Friesner, J. Tirado-Rives, W.L. Jorgensen, J. Phys. Chem. B 105 (2001) 6474–6487.
[49] D.P. Tieleman, J.L. Maccallum, W.L. Ash, C. Kandt, Z. Xu, L. Monticelli, J Phys Condens Matter 18 (2006) S1221–S1234.
[50] W.L. Jorgensen, J. Chandrasekhar, J.D. Madura, R.W. Impey, M.L. Klein, J. Chem. Phys. 79 (1983) 926.
[51] W. Kabsch, C. Sander, Biopolymers 22 (1983) 2577–2637.
[52] R.P. Joosten, T.A.H. Te Beek, E. Krieger, M.L. Hekkelman, R.W.W. Hooft, R. Schneider, C. Sander, G. Vriend, Nucleic acids research 39 (2011) D411–D419.
[53] W. Humphrey, A. Dalke, K. Schulten, Journal of molecular graphics 14 (1996) 33–38.
[54] http://www.ks.uiuc.edu/Research/vmd/.
[55] B. Bechinger, C. Aisenbrey, Current Protein and Peptide Science 13 (2012) 602–610.
[56] D. Sengupta, H. Leontiadou, A.E. Mark, S.J. Marrink, Biochim Biophys Acta 1778 (2008) 2308–2317.
[57] L.S. Vermeer, Y. Lan, V. Abbate, E. Ruh, T.T. Bui, L.J. Wilkinson, T. Kanno, E. Jumagulova, J. Kozlowska, J. Patel, C.A. McIntyre, W.C. Yam, G. Siu, R.A. Atkinson, J.K. Lam, S.S. Bansal, A.F. Drake, G.H. Mitchell, A.J. Mason, J Biol Chem 287 (2012) 34120–34133.
[58] M. Mihajlovic, T. Lazaridis, Biochim Biophys Acta 1818 (2012) 1274–1283.
[59] M. Mihajlovic, T. Lazaridis, Biochim Biophys Acta 1798 (2010) 1494–1502.
[60] F.-Y. Chen, M.-T. Lee, H.W. Huang, Biophysical journal 84 (2003) 3751–3758.
[61] G. Fuertes, D. Gimenez, S. Esteban-Martin, O.L. Sanchez-Munoz, J. Salgado, Eur Biophys J 40 (2011) 399–415.
[62] S.J. Marrink, E. Lindahl, O. Edholm, A.E. Mark, J. Am. Chem. Soc. 123 (2001) 8638–8639.
[63] C. Vega, J.L.F. Abascal, E. Sanz, L.G. MacDowell, C. McBride, J. Phys.: Condens. Matter 17 (2005) S3283–S3288.
[64] V.K. Mishra, M.N. Palgunachari, J.P. Segrest, G.M. Anantharamaiah, Journal of Biological Chemistry 269 (1994) 7185–7191.
[65] K. Hristova, W.C. Wimley, The Journal of membrane biology 239 (2011) 49–56.
[66] M.R. Yeaman, N.Y. Yount, Pharmacol Rev 55 (2003) 27–55.
[67] Z. Oren, J.C. Lerman, G.H. Gudmundsson, B. Agerberth, Y. Shai, Biochem J 341 (1999) 501–513.
[68] L. Silvestro, P.H. Axelsen, Biophysical journal 79 (2000) 1465–1477.